

Octupolar order and Ising quantum criticality tuned by strain and dimensionality: Application to d -orbital Mott insulators

Sreekar Voleti,^{1,*} Arijit Halder,^{1,†} and Arun Paramakanti^{1,‡}

¹*Department of Physics, University of Toronto, 60 St. George Street, Toronto, ON, M5S 1A7 Canada*

(Dated: January 1, 2023)

Recent experiments have discovered multipolar orders in a variety of d -orbital Mott insulators. Motivated by uncovering the exchange interactions which underlie octupolar order proposed in the osmate double perovskites, we study a two-site model using exact diagonalization on a five-orbital Hamiltonian, incorporating spin-orbit coupling (SOC) and interactions, and including both intra-orbital and inter-orbital hopping. Using an exact Schrieffer-Wolff transformation, we then extract an effective pseudospin Hamiltonian for the non-Kramers doublets, uncovering dominant ferroorbital coupling driven by the interplay of two distinct intra-orbital hopping terms. Using classical Monte Carlo simulations on the face-centered cubic lattice, we obtain a ferroorbital transition temperature which is in good agreement with experiments on the osmate double perovskites. We also explore the impact of uniaxial strain and dimensional tuning via ultrathin films, which are shown to induce a transverse field on the Ising octupolar order. This suppresses T_c and potentially allows one to access octupolar Ising quantum critical points. We discuss possible implications of our results for a broader class of materials which may host such non-Kramers doublet ions.

PACS numbers: 75.25.aj, 75.40.Gb, 75.70.Tj

I. INTRODUCTION

Multipolar orders have been extensively studied in f -electron compounds [1–16] where spin-orbit coupling and interactions dominate over weaker crystal field effects. However, there is growing evidence for such exotic “higher multipoles” in a wide range of heavy d -orbital metals such as LiOsO_3 and $\text{Cd}_2\text{Re}_2\text{O}_7$ which may exhibit odd-parity nematic orders [17, 18], or quadrupolar orders as proposed in A_2OsO_4 (with $\text{A} = \text{K, Rb, Cs}$) [19].

Recent work from various groups have also begun to explore such orders in the Mott insulator regime, where a local picture provides a useful starting point. For d -orbitals in an octahedral crystal field, the t_{2g} single particle levels are split by SOC, resulting in a four-fold degenerate, $j_{\text{eff}} = 3/2$, ground state and a doubly degenerate, $j_{\text{eff}} = 1/2$, excited state. These levels can realize interesting multipolar phases at different electron fillings. For instance, d^1 Mott insulators can realize the magnetism of $j_{\text{eff}} = 3/2$ spins. Theoretical studies of such moments on the FCC lattice have shown that they can lead to wide regimes of quadrupolar order in the phase diagram [20–22] which may coexist with conventional dipolar magnetic order, or valence bond orders [23]. Experiments on $5d^1$ oxides, $\text{Ba}_2\text{NaOsO}_6$ with Os^{7+} [24, 25] and $\text{Ba}_2\text{MgReO}_6$ with Re^{6+} [26], have found evidence for two phase transitions, with a higher temperature quadrupolar ordering transition followed by dipolar ordering at a lower temperature.

In this paper, we focus on d^2 Mott insulators, where [20, 21, 27, 28] have argued for a local $J = 2$ spin mo-

ment, which can lead to various exotic orders including quadrupolar phases. We have recently reexamined this issue [29] and shown that virtual excitations into the high energy e_g orbitals split the five-fold degeneracy of the $J = 2$ moment as $2(E_g) \oplus 3(T_{2g})$, resulting in a ground state non-Kramers E_g doublet carrying quadrupolar and octupolar moments. We had proposed, on phenomenological grounds, that ferro-octupolar (FO) order of these local moments provides a comprehensive understanding of the time-reversal breaking phase transition observed in the cubic ordered double perovskite (DP) Mott insulators, $\text{Ba}_2\text{ZnOsO}_6$, $\text{Ba}_2\text{CaOsO}_6$, and $\text{Ba}_2\text{MgOsO}_6$, which host a $5d^2$ configuration on Os [30–34]. It is tempting to speculate that this Ising ferro-octupolar order might provide a template for storing information. Interestingly, our theory of octupolar order is reminiscent of, but distinct from, an old proposal by van den Brink and Khomskii [35] of “complex e_g orbital” order in the colossal magnetoresistive manganites, which studied a possible time-reversal breaking order of the single-particle e_g orbitals.

Despite the seeming success of our phenomenological proposal, our previous work did not identify the microscopic origin of the octupolar order. A very recent study combining *ab initio* and dynamical mean field theory calculations [36] has found unequivocal evidence of FO exchange - however, the essential ingredients favoring octupolar order were not fully clarified in this work. At the same time, several competing theories have emerged for the phase transition observed in these osmates. One proposal argues for antiferro-octupolar ordering of the E_g doublets [37]. Other studies have argued for antiferro-quadrupolar orders based on a perturbative calculation of the exchange interactions including coupling to Jahn-Teller active phonons [38, 39]; these, however, relied on simplifying assumptions to permit analytical progress and they do not naturally explain the time-reversal sym-

* svoleti@physics.utoronto.ca

† arijit.halder@utoronto.ca

‡ arunp@physics.utoronto.ca

metry breaking observed in experiments. Motivated by these developments, we consider here a two-site five-orbital model, which we solve using numerical exact diagonalization. We explore the phase diagram as we vary the inter-orbital and intra-orbital hoppings, as well as inter-site Coulomb repulsion. Over a wide regime of parameters, we find ferro-octupolar order with robust high T_c , providing a microscopic explanation for the experimental observations on the double perovskite osmates. Furthermore, we investigate the impact of uniaxial strain on the effective model and show that this leads to a transverse field on the Ising octupolar order, allowing one to tune T_c and potentially access octupolar Ising quantum critical points. Our study builds on previous work showing strain-tuning of nematic (quadrupolar) order and its transverse field quantum criticality [40].

This paper is organized as follows. In Section II we discuss the single-site and two-site exact diagonalization results for the full five-orbital model, and show how we extract the pseudospin exchange model using an exact Schrieffer-Wolff transformation. Our results yield large swaths of parameter space with dominant FO exchange interactions on the face-centered cubic (FCC) lattice. In Section III, we discuss Monte Carlo simulations of this pseudospin model, and show that it leads to a phase transition into the FO ordered state with T_c in reasonable agreement with experiments on $\text{Ba}_2\text{ZnOsO}_6$, $\text{Ba}_2\text{CaOsO}_6$, and $\text{Ba}_2\text{MgOsO}_6$. Section IV considers the impact of uniaxial strain and dimensional tuning via thin films, showing that it leads to an effective transverse field on the Ising FO order, suppressing T_c and driving the system towards an Ising quantum critical point. Section V presents the summary and outlook.

II. EXTRACTING THE PSEUDOSPIN HAMILTONIAN

A. Single-site exact diagonalization study

The single-site model for the d^2 configuration incorporating both crystal-field effects, electron-electron interactions, and spin-orbit coupling, has been carefully explored in our previous work. To keep our discussion self-contained, we sketch the main results. We employ a single-site (local) Hamiltonian:

$$H_{\text{loc}} = H_{\text{CEF}} + H_{\text{SOC}} + H_{\text{int}} \quad (1)$$

which includes $t_{2g} - e_g$ crystal field splitting, SOC, and electronic interactions, written in the orbital basis ($\{yz, xz, xy\}, \{x^2-y^2, 3z^2-r^2\}\} \leftrightarrow (\{1, 2, 3\}, \{4, 5\})$ where $\alpha \equiv \{1, 2, 3\}$ label t_{2g} orbitals and $\alpha \equiv \{4, 5\}$ label e_g orbitals. The CEF term is given by:

$$H_{\text{CEF}} = V_C \sum_{\alpha=4,5} \sum_s n_{\alpha,s} \quad (2)$$

where s is the spin. The SOC term is

$$H_{\text{SOC}} = \frac{\lambda}{2} \sum_{\alpha,\beta} \sum_{s,s'} \langle \alpha | \mathbf{L} | \beta \rangle \cdot \langle s | \boldsymbol{\sigma} | s' \rangle c_{\alpha s}^\dagger c_{\beta s'} \quad (3)$$

where $\boldsymbol{\sigma}$ refers to the vector of Pauli matrices, and \mathbf{L} are orbital angular momentum matrices. The operators $c_{\alpha s}$, $c_{\alpha s}^\dagger$ and $n_{\alpha s}$ destroy, create, and count the electrons with spin s in orbital α . The Kanamori interaction is given by

$$H_{\text{int}} = U \sum_{\alpha} n_{\alpha\uparrow} n_{\alpha\downarrow} + \left(U' - \frac{J_H}{2} \right) \sum_{\alpha>\beta} n_{\alpha} n_{\beta} \quad (4)$$

$$- J_H \sum_{\alpha \neq \beta} \mathbf{S}_{\alpha} \cdot \mathbf{S}_{\beta} + J_H \sum_{\alpha \neq \beta} c_{\alpha\uparrow}^\dagger c_{\alpha\downarrow}^\dagger c_{\beta\downarrow} c_{\beta\uparrow}$$

where U and U' are the intra- and inter-orbital Hubbard interactions, J_H is the Hund's coupling, and $\mathbf{S}_{\alpha} = (1/2)c_{\alpha s}^\dagger \boldsymbol{\sigma}_{s,s'} c_{\alpha s'}$. The operator $n_{\alpha} \equiv n_{\alpha\uparrow} + n_{\alpha\downarrow}$ counts the total number of electrons in orbital α . Assuming spherical symmetry of the Coulomb interaction, we set $U' = U - 2J_H$ [41]. In this calculation, we use $V_C = 2.2$ eV, $\lambda = 0.4$ eV, $U = 2.5$ eV, and $J_H = 0.3$ eV in order to obtain a spin gap (described below) which matches values obtained by neutron studies [34].

When the crystal field splitting $V_C \rightarrow \infty$, it leads to a five-fold degenerate ground state corresponding to a spin-orbit coupled $J = 2$ quantum spin. For realistic finite V_C , this $J = 2$ manifold is split, leading to a non-Kramers pseudospin doublet, with wavefunctions given in terms of J_z eigenstates as:

$$|\psi_{g,\uparrow}\rangle = |0\rangle; \quad |\psi_{g,\downarrow}\rangle = \frac{1}{\sqrt{2}}(|2\rangle + |-2\rangle) \quad (5)$$

and an excited state triplet separated from the doublet by a gap ~ 20 meV. The states $|\psi_{g,\uparrow}\rangle, |\psi_{g,\downarrow}\rangle$ are individually time-reversal invariant. The angular momentum operators $(J_x^2 - J_y^2)/2\sqrt{3}$ and $-(3J_z^2 - J^2)/6$, restricted to this basis, act as Pauli matrices (τ_x, τ_z) , forming the two components of an XY-like quadrupolar order parameter, while $-\overline{J_x J_y J_z}/3$ (with overline denoting symmetrization) behaves as τ_y , and serves as the Ising-like octupolar order parameter. We will define the corresponding pseudospin-1/2 operators as $\tilde{S}_{\alpha} = \tau_{\alpha}/2$. The ferro-octupolar order discussed later corresponds to all pseudospins being in the state $|\psi_{\pm}^{\text{oct}}\rangle = |\psi_{g,\uparrow}\rangle \pm i|\psi_{g,\downarrow}\rangle$, with the signs reflecting the \mathbb{Z}_2 Ising character of octupolar order, and the factor of 'i' reflecting time-reversal symmetry breaking. Our next goal is to uncover the interaction between these pseudospins on neighboring sites.

B. Two-site exact diagonalization calculation

We consider a two-site model, with each site housing a non-Kramers doublet as described above. Two sites lying in the γ plane (where $\gamma \in \{xy, yz, zx\}$) are coupled via a hopping Hamiltonian of the form

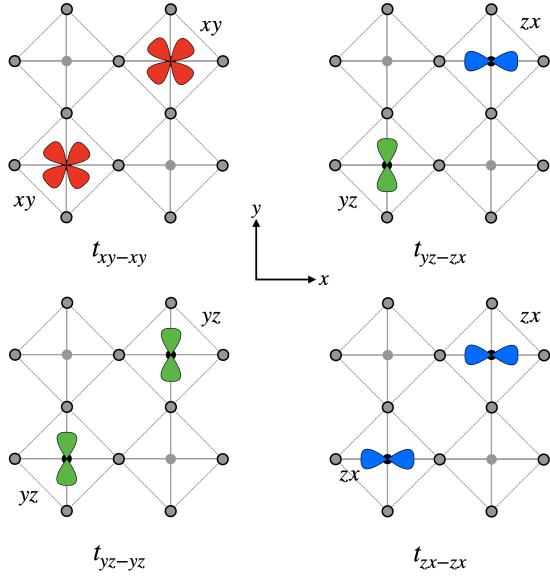


FIG. 1. Schematic top-view of orbitals in the xy plane showing different nearest-neighbor hoppings in the xy plane. The corresponding hoppings in the xz, yz planes are determined by the cubic point group symmetry.

$$H_T^\gamma = \sum_{\alpha\beta s} (T_{\alpha\beta}^\gamma c_{2\beta s}^\dagger c_{1\alpha s} + T_{\beta\alpha}^{\gamma\dagger} c_{1\alpha s}^\dagger c_{2\beta s}) \quad (6)$$

where T^γ is the hopping matrix in the γ plane. In the xy plane the sites are coupled via four hopping channels, as described in Fig. 1. The matrix in this plane takes the form

$$T^{xy} = \left(\begin{array}{ccc|cc} t_{yz-yz} & t_{yz-zx} & 0 & 0 & 0 \\ t_{zx-yz} & t_{zx-zx} & 0 & 0 & 0 \\ 0 & 0 & t_{xy-xy} & 0 & 0 \\ \hline 0 & 0 & 0 & 0 & 0 \\ 0 & 0 & 0 & 0 & 0 \end{array} \right). \quad (7)$$

With cubic symmetry, the corresponding matrices in the other planes can be obtained via C_3 transformations about the $[111]$ direction. The dominant hopping in the xy plane is t_{xy-xy} , which is larger than $t_{yz-zx} = t_{zx-yz}$, which in turn is larger than $t_{yz-yz} = t_{zx-zx}$. The two-site model can be studied in the Fock space sector with four d electrons having access to 20 distinct states (10 on each site). The dimension of the resulting Hilbert space is thus $\binom{20}{4} = 4845$. The two-site Hamiltonian

$$H^\gamma = H_{\text{loc}} \otimes \mathcal{I} + \mathcal{I} \otimes H_{\text{loc}} + H_T^\gamma \quad (8)$$

consists of two copies of the single-site Hamiltonian presented in Eq. 1, in addition to H_T^γ . The symbol \mathcal{I} denotes the identity operator for the Hilbert space in the single-site problem.

C. Exact Schrieffer-Wolff transformation to obtain the pseudospin Hamiltonian

We compute the effective pseudospin Hamiltonian in the presence of intersite couplings using an exact Schrieffer-Wolff (SW) transformation [42, 43]. SW transformations in general are used to obtain effective low-energy description of a “perturbed” Hamiltonian in terms of the low-energy eigenstates of the original “unperturbed” Hamiltonian. This is accomplished by defining a so called direct rotation [43] that connects the low-energy subspaces of the “unperturbed” and “perturbed” Hamiltonians.

For our two-site model, the intersite hoppings in Eq. 6 will serve as the source of the perturbation. Therefore, we consider the two-site decoupled Hamiltonian (Eq. 8 without H_T^γ) as the unperturbed Hamiltonian H_0 and the coupled model H^γ (Eq. 8) as the perturbed Hamiltonian. As already discussed (Sec. II A), the low-energy subspace of the single-site Hamiltonian has a two-fold degeneracy, which translates to a four-dimensional degenerate subspace for the decoupled two-site Hamiltonian H_0 . We refer to this subspace for the decoupled (unperturbed) Hamiltonian as \mathcal{P}_0 . Upon introducing intersite couplings, the subspace \mathcal{P}_0 gets modified perturbatively to a different four-dimensional subspace \mathcal{P} . This new subspace \mathcal{P} is by definition the low-energy eigenspace for the coupled two-site Hamiltonian H^γ .

The SW transformation that rotates the subspace \mathcal{P} to \mathcal{P}_0 is defined as the unitary transformation

$$U_{\mathcal{P} \rightarrow \mathcal{P}_0} = \sqrt{(2P_0 - \mathbf{1})(2P - \mathbf{1})}, \quad (9)$$

where $P = \sum_{\phi \in \mathcal{P}} |\phi\rangle \langle \phi|$, $P_0 = \sum_{\psi_0 \in \mathcal{P}_0} |\psi_0\rangle \langle \psi_0|$ are the projection operators onto the subspace \mathcal{P} and \mathcal{P}_0 respectively, and $\mathbf{1}$ is the identity operator. The square root in Eq. 9 is defined using a branch cut on the complex plane such that $\sqrt{1} = 1$. The states $\{|\phi\rangle\}$ denote a choice of basis spanning \mathcal{P} and $\{|\psi\rangle\}$ is a basis for \mathcal{P}_0 . The operator $U_{\mathcal{P} \rightarrow \mathcal{P}_0}$ by construction maps a state $|\phi\rangle \in \mathcal{P}$ to a unique state $|\psi\rangle \in \mathcal{P}_0$, such that $U_{\mathcal{P} \rightarrow \mathcal{P}_0} |\phi\rangle = |\psi\rangle$. Consequently, $U_{\mathcal{P} \rightarrow \mathcal{P}_0}^\dagger$ does the opposite, i.e., $U_{\mathcal{P} \rightarrow \mathcal{P}_0}^\dagger |\psi\rangle = |\phi\rangle$. Furthermore, $U_{\mathcal{P} \rightarrow \mathcal{P}_0}$ is guaranteed to be unique iff $U_{\mathcal{P} \rightarrow \mathcal{P}_0}^2$, i.e. $(2P_0 - \mathbf{1})(2P - \mathbf{1})$, does not have any eigenvalues that reside on the negative real axis of the complex plane. It has been shown [43] that this is indeed the case when the corrections arising from the perturbation are sufficiently small compared with the spectral-gap Δ separating the low-energy subspace \mathcal{P}_0 from the excited states of the unperturbed Hamiltonian H_0 . For our two-site model, as discussed below, we have checked that the perturbative level-shifts are weak compared with the spectral-gap Δ separating the non-Kramer’s doublet (Eq. 5) from rest of the spectrum, justifying a pseudospin-1/2 model of the low energy two-site spectrum.

Usually a direct computation of $U_{\mathcal{P} \rightarrow \mathcal{P}_0}$ (see Eq. 9) is extremely difficult in a many-body setting, since a

full computation of the perturbed subspace \mathcal{P} , spanning all orders of perturbation, is hard due to the exponential complexity of the many-body problem. Therefore, a series expansion for $U_{\mathcal{P} \rightarrow \mathcal{P}_0}$ in powers of perturbation strength is often used as an approximation. However, for our two-site problem the dimension of the many-body Fock space is 4845 (see discussion above Eq. 8), and well within reach of exact diagonalization (ED) techniques. This allows us to solve for the low energy subspace \mathcal{P} (\mathcal{P}_0) for the perturbed (unperturbed) Hamiltonian exactly, and obtain $U_{\mathcal{P} \rightarrow \mathcal{P}_0}$ using Eq. 9 to all orders of perturbation in intersite couplings.

We then use the computed SW transformation $U_{\mathcal{P} \rightarrow \mathcal{P}_0}$ to obtain the effective low energy form of the perturbed Hamiltonian H^γ in the original subspace \mathcal{P}_0 of the unperturbed problem, as follows

$$H_{\text{eff}}^\gamma = (P_0 U_{\mathcal{P} \rightarrow \mathcal{P}_0}) H^\gamma (U_{\mathcal{P} \rightarrow \mathcal{P}_0}^\dagger P_0). \quad (10)$$

Since we use the exact SW transformation $U_{\mathcal{P} \rightarrow \mathcal{P}_0}$ to compute H_{eff}^γ , the resulting 4×4 Hamiltonian is also exact in the sense that it has contributions from all orders of perturbation. By construction, the eigenvalues of H_{eff}^γ are precisely equal to the lowest four eigenvalues of H^γ .

Having proposed the strategy to extract H_{eff}^γ , we need to compute the effective 4×4 Hamiltonian in a basis that will naturally allow us to interpret H_{eff}^γ in the form of a valid pseudospin Hamiltonian. Therefore, we carry out the entire computation discussed above, using a basis spanning \mathcal{P}_0 in which the operators $(J_x^2 - J_y^2)$, $-J_x J_y J_z$, $(3J_z^2 - J^2)$ on sites $i = 1, 2$, admit the Pauli matrix representations $\tau_x \otimes \tau_0$, $\tau_y \otimes \tau_0$, $\tau_z \otimes \tau_0$ and $\tau_0 \otimes \tau_x$, $\tau_0 \otimes \tau_y$, $\tau_0 \otimes \tau_z$, respectively, where τ_0 is the 2×2 identity matrix. The steps that go into selecting such a basis for \mathcal{P}_0 are discussed in App. A. The resulting pseudospin Hamiltonian of the γ plane in this basis takes the general form:

$$H_{\text{spin}}^\gamma = \tilde{\mathbf{S}}_1^\top \mathcal{K}^\gamma \tilde{\mathbf{S}}_2 + \mathbf{h}_1^\gamma \cdot \tilde{\mathbf{S}}_1 + \mathbf{h}_2^\gamma \cdot \tilde{\mathbf{S}}_2, \quad (11)$$

where the symbols $\tilde{\mathbf{S}}_{i=1,2} \equiv [\tilde{S}_{ix}, \tilde{S}_{iy}, \tilde{S}_{iz}]$ represent the pseudospin operators for the two sites $i = 1, 2$. The effective “spin-spin” interactions are encoded in the 3×3 \mathcal{K}^γ tensor and \mathbf{h}_i^γ are effective time-reversal even “Zeeman” fields acting on the pseudospins. Both, the \mathcal{K}^γ tensor and the components of the fields \mathbf{h}_i^γ , can be obtained from the exactly computed H_{eff}^γ as follows

$$\begin{aligned} \mathcal{K}_{\alpha\beta}^\gamma &= \text{Tr} [H_{\text{eff}}^\gamma (\tau_\alpha \otimes \tau_\beta)] \\ (\mathbf{h}_1^\gamma)_\alpha &= \text{Tr} [H_{\text{eff}}^\gamma (\tau_\alpha \otimes \tau_0)]/2 \\ (\mathbf{h}_2^\gamma)_\alpha &= \text{Tr} [H_{\text{eff}}^\gamma (\tau_0 \otimes \tau_\alpha)]/2 \end{aligned}$$

While the “Zeeman” fields appear to break the cubic symmetry of the lattice, they appear precisely because we consider one bond at a time (Fig. 1, for example, shows only the bond in the xy plane), a process which does not respect cubic symmetry. When summed over all the neighbours of the FCC lattice, the net field vanishes

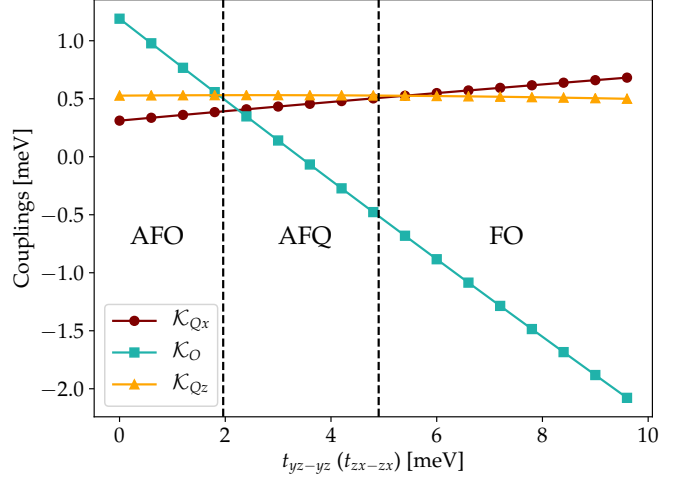


FIG. 2. Evolution of couplings in xy plane as a function of the intra-orbital yz - yz and zx - zx hopping. The dashed lines show the phases based on the most dominant couplings. This cut was made for $t_{xy-xy} = -150$ meV and $t_{yz-zx} = 30$ meV.

exactly, i.e.

$$\sum_{\gamma \in \{xy, yz, zx\}} \mathbf{h}_i^\gamma = 0,$$

thus restoring the full symmetry. In Sec. IV, we will consider the impact of uniaxial strain, which will give rise to situations where the net “Zeeman” field on the pseudospin does not vanish (which is to be expected, since the strain explicitly breaks cubic symmetry and intersite couplings can then lift the pseudospin degeneracy).

D. Exchange Couplings

The symmetry considerations outlined in App. B dictate that the pseudospin Hamiltonian in the xy plane is an XYZ model:

$$H_{\text{spin}}^{xy} = \mathcal{K}_{Qx} \tilde{S}_{1x} \tilde{S}_{2x} + \mathcal{K}_{Qz} \tilde{S}_{1z} \tilde{S}_{2z} + \mathcal{K}_O \tilde{S}_{1y} \tilde{S}_{2y}, \quad (12)$$

where \mathcal{K}_{Qx} and \mathcal{K}_{Qz} are the quadrupole-quadrupole couplings, and \mathcal{K}_O is the octupole-octupole coupling. For bonds in other planes, the exchange couplings may be obtained using C_3 rotations about the (111) axis, and they involve off-diagonal symmetric couplings of the form $(\tilde{S}_{1x} \tilde{S}_{2z} + \tilde{S}_{1z} \tilde{S}_{2x})$. In this section, we will drop the Zeeman field terms from Eq. 11, since they cancel out upon summing over all neighbors as outlined at the end of Sec. II C. Keeping the dominant t_{xy-xy} hopping fixed at -150 meV, we vary t_{yz-zx} and $t_{yz-yz} = t_{zx-zx}$ in the ranges $0-30$ meV and $0-10$ meV, respectively, to study the dominant order hosted by the pseudospin models. We do so by analyzing the dependence of the couplings, \mathcal{K}_{Qx} , \mathcal{K}_{Qz} and \mathcal{K}_O on the hopping terms t_{yz-yz} and t_{yz-zx} . Fig. 2 shows a representative example of this analysis

when $t_{yz-zx} = 30$ meV. As a first pass at identifying the phases in the model, we simply assign phases based on the dominant coupling in the XYZ model - an approach that will be corroborated below by classical Monte Carlo simulations in Sec. III. The three phases that appear in this phase diagram spanned by the subdominant hoppings are:

1. Ferro-Octupolar (FO) : $\mathcal{K}_O < 0$
2. Antiferro-Octupolar (AFO) : $\mathcal{K}_O > 0$
3. Antiferro-Quadrupolar (AFQ) : $\mathcal{K}_{Q\alpha} > 0$ ($\alpha \in \{x, z\}$)

In Fig. 3(a), we lay out the full phase diagram in the $t_{yz-yz} - t_{yz-zx}$ plane and label the phases appropriately by identifying the dominant coupling. Interestingly, we see that the FO phase forms the largest and most robust swath of the phase diagram centered around Fig. 3(a). Previous proposals have argued for the stabilization of both AFO and AFQ phases, and while these phase do exist in our model, we will show in Sec. III that for the reasonable choice of hopping parameters used, they have critical temperatures that are incompatible with experimental evidence. The specific quadrupolar ordering patterns coming from these frustrated interactions have been explored in previous works [37, 38].

III. MONTE CARLO SIMULATIONS ON THE FACE-CENTERED CUBIC LATTICE

In this section, we discuss the phase diagram of the pseudospin-1/2 Hamiltonian in Eq. 12, with coupling constants derived from microscopics, by treating the pseudospins as classical moments, and using Monte Carlo (MC) simulations to extract their ordering and thermal phase transitions. Such an approach is expected to qualitatively capture the phase diagram on the three-dimensional face-centered cubic lattice of the ordered double perovskites; quantum fluctuations may lead to quantitative corrections to the phase boundaries and transition temperatures.

The simulations were conducted using the SpinMC package [44] on a cluster of 1331 spins ($11 \times 11 \times 11$ primitive FCC cluster) with periodic boundary conditions. To construct a phase diagram, pseudospin Hamiltonians were generated using a fixed dominant hopping $t_{xy-xy} = -150$ meV, and varying t_{yz-zx} and t_{yz-yz} in the ranges 0–30 meV and 0–20 meV, respectively (DFT studies on these and other 5d double perovskites have shown that these are reasonable choices [39, 45]). We observe, in each case, a single thermal phase transition corresponding to a sharp peak in the specific heat C_V of the system, and accompanied by the development of a nonzero order parameter as illustrated for a ferro-octupolar transition in Fig. 4. This representative plot was generated using hopping parameters close to

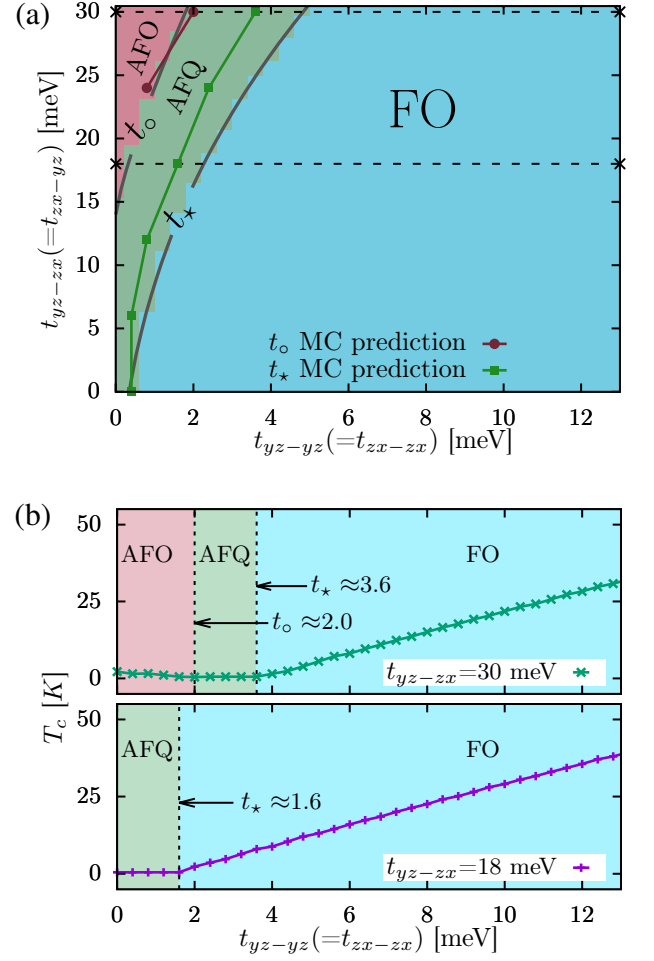


FIG. 3. (a) Phase diagram in subdominant hopping parameter space, using a fixed $t_{xy-xy} = -150$ meV. The solid black phase boundaries t_o and t_* denote the AFO-AFQ and AFQ-FO phase transition boundaries calculated simply by considering the dominant coupling (as outlined in Sec. II D). The colored lines (represented with symbols \bullet , \blacksquare) denote the phase boundaries obtained from Monte Carlo (MC) simulations (as outlined in Sec. III). The MC predictions of the t_* boundary occur at smaller values of t_{yz-zx} , likely because the frustration of the quadrupoles on the FCC lattice causes the unfrustrated ferro-octupolar (FO) order to be preferentially stabilized despite the coupling having a smaller magnitude. (b) Representative cuts along the y -axis of the phase diagram (denoted as dashed-horizontal lines in (a)), showing the evolution of the critical temperature T_c with t_{yz-yz} . Three piecewise regions, representing the indicated phases, can be observed. It can be seen that the values of T_c for the AFO and AFQ phases are far lower than the T_c values of 30–50 K reported in experiments, while the T_c for the FO phase fits well with experiments.

those recently obtained using Density Functional Theory (DFT) calculations [39] on the osmate double perovskites.

To identify phase boundaries shown in the full phase diagram in Fig. 3(a), we look at the development of the critical temperature T_c as a function of the hoppings

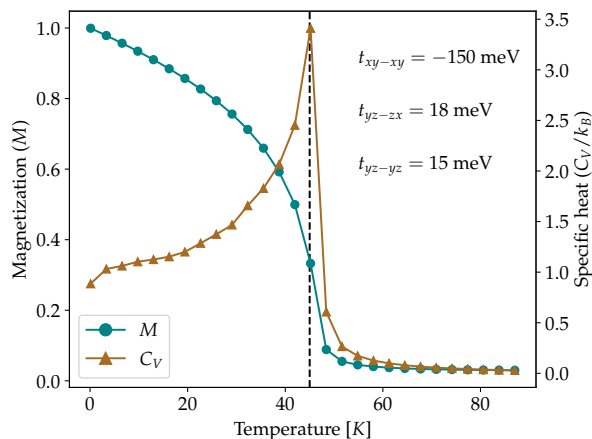


FIG. 4. Representative example of Monte Carlo simulation, for the hopping parameters corresponding to the Ferro-Octupolar (FO) phase. It can be seen that there is a single phase transition, characterized by a peak in the specific heat (C_V) and the magnetization (ferromagnetic order parameter) becoming non vanishing.

t_{yz-zx} and t_{yz-yz} (see Fig. 3(b)), and identify kinks, suggesting a change in the underlying analytic form of the dependence. The phase boundaries (shown with solid-lines and symbols in Fig. 3(a)) obtained using this method match well with the “naïve” method of computing the phase boundaries (t_o , t_* in Fig. 3(a)) described in Sec. IID, where we simply looked at the dominant term in the pseudospin Hamiltonian.

IV. TUNING OCTUPOLAR ORDER VIA UNIAXIAL STRAIN OR DIMENSIONALITY

The multipolar orders we have obtained above are highly sensitive to the nature of the inter-orbital and intra-orbital hoppings as discussed above. In addition, we have seen that the full cubic point group symmetry leads to a cancellation of the time-reversal even “field” terms acting on the (τ_x, τ_z) pseudospin components, leaving us with only two-spin exchange terms. Motivated by tuning the multipolar orders, we next consider the impact of breaking cubic symmetry via strain or interfaces on the pseudospin Hamiltonian.

Uniaxial strain: For simplicity, we consider uniaxial strain along the (001) axis (z -axis), which we take into account by rescaling all the inter-site hoppings for neighbors in the xz and yz planes by a factor $(1 - \delta)$, with $\delta > 0$ corresponding to tensile strain and $\delta < 0$ corresponding to compressive strain. Given the typical strong dependence of the hopping amplitudes on the lattice constants [46, 47], we expect the lattice strain $\varepsilon_{zz} \ll \delta$. A careful account of strain effects must rely on experiments and *ab initio* electronic structure calculations, in order to relate δ to changes in lattice constants, and to examine changes in the relative strengths of the inter-orbital and

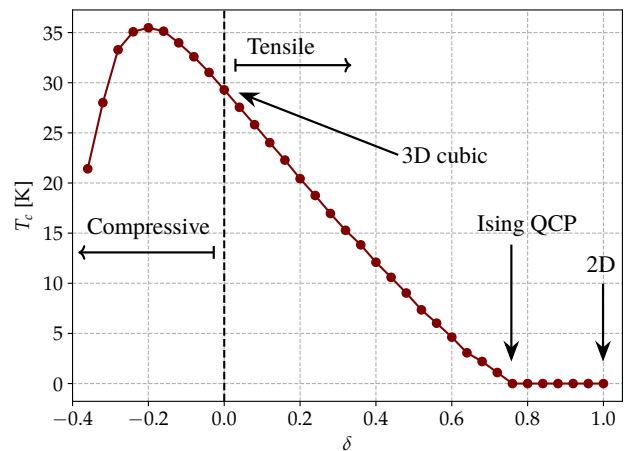


FIG. 5. Evolution of the critical temperature, T_c as a function of the relative tensile distortion δ . The hopping parameters used here are $t_{yz-zx} = 18$ meV, $t_{yz-yz} = 10$ meV.

intra-orbital terms; we defer this to a future study. We repeat the two-site exact diagonalization and Schrieffer-Wolff procedure as a function of δ , and find that $\delta \neq 0$ leads to a non-cancelling “field” acting on the (τ_x, τ_z) pseudospin components due to loss of cubic symmetry. This “field” is transverse to the octupolar ordering direction τ_y , and can thus induce quantum fluctuations which can suppress $\langle \tau_y \rangle$, and reveal a three-dimensional (3D) octupolar Ising quantum critical point.

Fig. 5 shows the computed T_c using the modified exchange couplings and induced “Zeeman field” in the presence of strain. We find that tensile strain ($\delta > 0$) leads to a strong suppression of T_c , due to combined effect of the weakening of octupolar exchange interactions in the yz, zx planes and the generated transverse field. On the other hand, for compressive strain ($\delta < 0$), T_c first increases, since the enhancement of the octupolar exchange coupling is initially more significant than the generated transverse field, before it begins to drop. For tensile strain, we find a (mean-field) 3D Ising quantum critical point at $\delta_c \approx 0.8$, beyond which the octupolar ordering is suppressed. While this critical point δ_c is at too large a value to be accessible in experiments, the δ -dependence of T_c at smaller strain may be explored in experiments.

Ultrathin films: The generation of “Zeeman fields” when symmetry is lowered from cubic also happens naturally at surfaces or interfaces. In particular, let us consider an ultrathin (001) epitaxial film where the top and bottom faces experience a field $\propto \tau_z$ due to reduced symmetry. If this surface field is sufficiently strong, and the film thickness is sufficiently small, the transverse surface field can polarize the bulk and kill the octupolar order in the entire 2D film. As an extreme limit, let us consider a monolayer film which conveniently corresponds to the limit $\delta \rightarrow 1$ of the uniaxial strain, when individual 2D layers of the FCC lattice completely decouple. In this 2D limit, Fig. 5 shows that octupolar order is absent, while octupolar ordering is present in the bulk. We thus

see that as we decrease the film thickness, we will tune the system through a 2D Ising quantum critical point. This is a more promising avenue to suppress T_c , and it would be extremely interesting to experimentally search for signatures of film-thickness dependent tuning through an octupolar quantum critical point.

Previous work has shown that shear strain can act as a transverse field on Ising nematic order and drive a nematic quantum phase transition [40]. Our work generalizes this idea to the case of octupolar order. Our work also goes beyond previous studies which have explored the interplay of weak magnetic field and strain for probes of octupolar ordering or octupolar susceptibility [16, 48].

V. DISCUSSION

We have discovered the key microscopic ingredients which underlie ferro-octupolar order in the ordered double perovskite osmates $\text{Ba}_2\text{ZnOsO}_6$, $\text{Ba}_2\text{CaOsO}_6$, and $\text{Ba}_2\text{MgOsO}_6$. Our calculations, which use exact diagonalization and an exact Schrieffer-Wolff transformation and Monte Carlo simulations, find that we can capture the octupolar order and its high transition temperature as observed in experiments. In addition, we have shown how strain can suppress the octupolar ordering temperature, potentially revealing an Ising quantum critical point. Our work has implications for a broad class of materials, including d -orbital transition metal oxides and f -orbital heavy fermion systems, where such multipolar orders may be accessible. For instance, NpO_2 is a well-known example of an fcc lattice material which hosts higher-rank multipolar order with time-reversal symmetry breaking [1–6]. Octupolar order of the T_{xyz} type explored here has also been proposed in the $\text{Pr}(\text{Ti,V,Ir})_2(\text{Al,Zn})_{20}$ compounds where Pr moments live on the diamond lattice [15, 16]. In future work, it would be important to extend our work to understand the origins of multipolar order in these materials, and explore the impact of strain and thin film geometries. More broadly, the impact of thin film geometries, surfaces, and interfaces, in promoting or suppressing multipolar orders in non-Kramers doublet systems appears to be a wide open field of study.

Note added: During completion of this manuscript, we became aware of the recent preprint by Churchill and Kee [39] which has partial overlap with our work. Mainly, these authors identify the combination of two different intra-orbital hoppings as favoring octupolar order, as we also independently discovered in our work. However, in significant contrast to our results which finds wide regimes of octupolar order, they find evidence for only dominant quadrupolar orders; we suspect this may arise from ignoring the Hund’s coupling in deriving the exchange Hamiltonian. These quadrupolar orders do not naturally account for the broken time-reversal symmetry observed in the osmate double perovskites.

VI. ACKNOWLEDGMENTS

We thank F. Lasse Buessen for useful discussions on the Monte Carlo simulations. This work was supported by the Natural Sciences and Engineering Research Council of Canada. Exact diagonalization computations were performed on the Niagara supercomputer at the SciNet HPC Consortium. SciNet is funded by: the Canada Foundation for Innovation; the Government of Ontario; Ontario Research Fund - Research Excellence; and the University of Toronto. Monte Carlo simulations were conducted on the Cedar supercomputer, one of Compute Canada’s National systems, located in Simon Fraser University.

Appendix A: Choosing \mathcal{P}_0 basis states in the Schrieffer-Wolff (SW) process

An important step in the SW process is ensuring that we use basis states for \mathcal{P}_0 which can be interpreted as direct products of (pseudo)spin states on the two sites. This enables us to interpret the extracted pseudospin Hamiltonian as an direct-product type interaction between the multipole moments in the doublet manifold. While there are many ways to do this, the simplest is to leverage the fact that the \mathcal{P}_0 Hamiltonian is decoupled, meaning that the basis states can be constructed out of the single site states.

At a single site level, we can ensure that the “up” and “down” pseudospin states from Sec. II A correspond to eigenstates of τ_z ($\propto 3J_z^2 - J^2$), by adding a term to the Hamiltonian which couples an infinitesimal magnetic field to this operator. This weakly breaks the two-fold degeneracy and the basis states of \mathcal{P}_0 can simply be built using the direct product of the aforementioned states.

Appendix B: Symmetry considerations for the Pseudospin Hamiltonian

As stated in the main text, the following correspondence exists between $J = 2$ angular momentum multipole moments and the Pauli matrices in the low energy non-Kramers doublet manifold:

$$\begin{aligned} \frac{1}{2\sqrt{3}}(J_x^2 - J_y^2) &\rightarrow \tau_x \\ -\frac{1}{3}\overline{J_x J_y J_z} &\rightarrow \tau_y \\ -\frac{1}{6}(3J_z^2 - J^2) &\rightarrow \tau_z \end{aligned} \quad (\text{B1})$$

Therefore, the most general spin-1/2 Hamiltonian takes the form (sites are numbered 1 and 2):

$$H_{\text{spin}} = \frac{1}{4}\mathcal{K}_{ab}(\tau_a \otimes \tau_b). \quad (\text{B2})$$

For a bond in the xy plane, the following symmetry considerations heavily constrain the form of \mathcal{K} :

1. Inversion symmetry about the center of the bond exchanges the site indices, implying that \mathcal{K} is symmetric, i.e.

$$\begin{aligned}\mathcal{K}_{xy} &= \mathcal{K}_{yz} \\ \mathcal{K}_{yz} &= \mathcal{K}_{zy} \\ \mathcal{K}_{zx} &= \mathcal{K}_{xz}\end{aligned}\quad (\text{B3})$$

2. Under the M_z mirror transformation (the mirror plane is $z = 0$), we have

$$\left. \begin{aligned} J_z &\rightarrow -J_z \\ J_x &\rightarrow -J_y \\ J_y &\rightarrow -J_x \end{aligned} \right\} \Rightarrow \left\{ \begin{aligned} \tau_x &\rightarrow -\tau_x \\ \tau_y &\rightarrow -\tau_y \\ \tau_z &\rightarrow \tau_z \end{aligned} \right. \quad (\text{B4})$$

For the above to be a symmetry of the system, we must have that $\mathcal{K}_{zx} = \mathcal{K}_{yz} = 0$

3. The system is time-reversal symmetric. Under the time reversal operation we have the following transformations:

$$\begin{aligned}\tau_y &\rightarrow -\tau_y \\ \tau_x, \tau_z &\rightarrow \tau_x, \tau_z\end{aligned}\quad (\text{B5})$$

This implies that $\mathcal{K}_{xy} = \mathcal{K}_{yz} = 0$

The above points, when considered together, lead to the vanishing of all the off-diagonal elements in \mathcal{K} . This leaves us with an XYZ Hamiltonian of the form

$$\mathcal{K} = \begin{pmatrix} \mathcal{K}_{xx} & 0 & 0 \\ 0 & \mathcal{K}_{yy} & 0 \\ 0 & 0 & \mathcal{K}_{zz} \end{pmatrix}. \quad (\text{B6})$$

In the main text, we have renamed $\mathcal{K}_{xx} \rightarrow \mathcal{K}_{Qx}$, $\mathcal{K}_{yy} \rightarrow \mathcal{K}_O$, and $\mathcal{K}_{zz} \rightarrow \mathcal{K}_{Qz}$. The exchange Hamiltonian in the zx and yz planes can be conveniently obtained using C_3 rotations about the cubic (111) direction.

-
- [1] P. Santini, S. Carretta, G. Amoretti, R. Caciuffo, N. Magnani, and G. H. Lander, *Rev. Mod. Phys.* **81**, 807 (2009).
 - [2] K. Haule and G. Kotliar, *Nature Physics* **5**, 796 EP (2009).
 - [3] P. Santini and G. Amoretti, *Phys. Rev. Lett.* **85**, 2188 (2000).
 - [4] J. A. Paixão, C. Detlefs, M. J. Longfield, R. Caciuffo, P. Santini, N. Bernhoeft, J. Rebizant, and G. H. Lander, *Phys. Rev. Lett.* **89**, 187202 (2002).
 - [5] A. Kiss and P. Fazekas, *Phys. Rev. B* **68**, 174425 (2003).
 - [6] Y. Tokunaga, D. Aoki, Y. Homma, S. Kambe, H. Sakai, S. Ikeda, T. Fujimoto, R. E. Walstedt, H. Yasuoka, E. Yamamoto, A. Nakamura, and Y. Shiokawa, *Phys. Rev. Lett.* **97**, 257601 (2006).
 - [7] T.-h. Arima, *Journal of the Physical Society of Japan* **82**, 013705 (2013).
 - [8] A. Sakai and S. Nakatsuji, *Journal of the Physical Society of Japan* **80**, 063701 (2011).
 - [9] T. J. Sato, S. Ibuka, Y. Nambu, T. Yamazaki, T. Hong, A. Sakai, and S. Nakatsuji, *Phys. Rev. B* **86**, 184419 (2012).
 - [10] M. Tsujimoto, Y. Matsumoto, T. Tomita, A. Sakai, and S. Nakatsuji, *Phys. Rev. Lett.* **113**, 267001 (2014).
 - [11] H.-H. Kung, R. E. Baumbach, E. D. Bauer, V. K. Thorsmølle, W.-L. Zhang, K. Haule, J. A. Mydosh, and G. Blumberg, *Science* **347**, 1339 (2015).
 - [12] H.-H. Kung, S. Ran, N. Kanchanavatee, V. Krapivin, A. Lee, J. A. Mydosh, K. Haule, M. B. Maple, and G. Blumberg, *Phys. Rev. Lett.* **117**, 227601 (2016).
 - [13] K. Hattori and H. Tsunetsugu, *Journal of the Physical Society of Japan* **85**, 094001 (2016).
 - [14] F. Freyer, J. Attig, S. Lee, A. Paramekanti, S. Trebst, and Y. B. Kim, *Phys. Rev. B* **97**, 115111 (2018).
 - [15] S. Lee, S. Trebst, Y. B. Kim, and A. Paramekanti, *Phys. Rev. B* **98**, 134447 (2018).
 - [16] A. S. Patri, A. Sakai, S. Lee, A. Paramekanti, S. Nakatsuji, and Y. B. Kim, *Nature Communications* **10**, 4092 (2019).
 - [17] L. Fu, *Phys. Rev. Lett.* **115**, 026401 (2015).
 - [18] J. W. Harter, Z. Y. Zhao, J.-Q. Yan, D. G. Mandrus, and D. Hsieh, *Science* **356**, 295 (2017), <https://science.sciencemag.org/content/356/6335/295.full.pdf>.
 - [19] S. Hayami, H. Kusunose, and Y. Motome, *Phys. Rev. B* **97**, 024414 (2018).
 - [20] G. Chen, R. Pereira, and L. Balents, *Phys. Rev. B* **82**, 174440 (2010).
 - [21] G. Chen and L. Balents, *Phys. Rev. B* **84**, 094420 (2011).
 - [22] C. Svoboda, W. Zhang, M. Randeria, and N. Trivedi, *Phys. Rev. B* **104**, 024437 (2021).
 - [23] J. Romhányi, L. Balents, and G. Jackeli, *Phys. Rev. Lett.* **118**, 217202 (2017).
 - [24] L. Lu, M. Song, W. Liu, A. P. Reyes, P. Kuhns, H. O. Lee, I. R. Fisher, and V. F. Mitrović, *Nature Communications* **8**, 14407 EP (2017).
 - [25] W. Liu, R. Cong, E. Garcia, A. Reyes, H. Lee, I. Fisher, and V. Mitrović, *Physica B: Condensed Matter* **536**, 863 (2018).
 - [26] D. Hirai and Z. Hiroi, *Journal of the Physical Society of Japan* **88**, 064712 (2019).
 - [27] C. Svoboda, M. Randeria, and N. Trivedi, *Phys. Rev. B* **95**, 014409 (2017).
 - [28] S. W. Lovesey, D. D. Khalyavin, G. van der Laan, and G. J. Nilsen, *Phys. Rev. B* **103**, 104429 (2021).
 - [29] A. Paramekanti, D. D. Maharaj, and B. D. Gaulin, *Phys. Rev. B* **101**, 054439 (2020).
 - [30] C. M. Thompson, J. P. Carlo, R. Flacau, T. Aharen, I. A. Leahy, J. R. Pollicemi, T. J. S. Munsie, T. Medina, G. M. Luke, J. Munevar, S. Cheung, T. Goko, Y. J. Uemura, and J. E. Greedan, *Journal of Physics: Condensed Matter* **26**, 306003 (2014).
 - [31] E. Kermarrec, C. A. Marjerrison, C. M. Thompson, D. D.

- Maharaj, K. Levin, S. Kroeker, G. E. Granroth, R. Flacau, Z. Yamani, J. E. Greedan, and B. D. Gaulin, *Phys. Rev. B* **91**, 075133 (2015).
- [32] C. M. Thompson, C. A. Marjerrison, A. Z. Sharma, C. R. Wiebe, D. D. Maharaj, G. Sala, R. Flacau, A. M. Hallas, Y. Cai, B. D. Gaulin, G. M. Luke, and J. E. Greedan, *Phys. Rev. B* **93**, 014431 (2016).
- [33] C. A. Marjerrison, C. M. Thompson, A. Z. Sharma, A. M. Hallas, M. N. Wilson, T. J. S. Munsie, R. Flacau, C. R. Wiebe, B. D. Gaulin, G. M. Luke, and J. E. Greedan, *Phys. Rev. B* **94**, 134429 (2016).
- [34] D. D. Maharaj, G. Sala, M. B. Stone, E. Kermarrec, C. Ritter, F. Fauth, C. A. Marjerrison, J. E. Greedan, A. Paramakanti, and B. D. Gaulin, *Phys. Rev. Lett.* **124**, 087206 (2020).
- [35] J. van den Brink and D. Khomskii, *Phys. Rev. B* **63**, 140416 (2001).
- [36] L. V. Pourovskii, D. F. Mosca, and C. Franchini, “Ferro-octupolar order and low-energy excitations in d^2 double perovskites of osmium,” (2021), [arXiv:2107.04493 \[cond-mat.str-el\]](https://arxiv.org/abs/2107.04493).
- [37] S. W. Lovesey and D. D. Khalyavin, *Phys. Rev. B* **102**, 064407 (2020).
- [38] G. Khaliullin, D. Churchill, P. P. Stavropoulos, and H.-Y. Kee, *Phys. Rev. Research* **3**, 033163 (2021).
- [39] D. Churchill and H.-Y. Kee, “Two quadrupolar orders in osmium double-perovskites,” (2021), [arXiv:2109.08104 \[cond-mat.str-el\]](https://arxiv.org/abs/2109.08104).
- [40] A. V. Maharaj, E. W. Rosenberg, A. T. Hristov, E. Berg, R. M. Fernandes, I. R. Fisher, and S. A. Kivelson, *Proceedings of the National Academy of Sciences* **114**, 13430 (2017), <https://www.pnas.org/content/114/51/13430.full.pdf>.
- [41] A. Georges, L. d. Medici, and J. Mravlje, *Annual Review of Condensed Matter Physics* **4**, 137 (2013).
- [42] J. R. Schrieffer and P. A. Wolff, *Phys. Rev.* **149**, 491 (1966).
- [43] S. Bravyi, D. P. DiVincenzo, and D. Loss, *Annals of Physics* **326**, 2793 (2011).
- [44] F. L. Buessen, “Spinmc.jl: Classical monte carlo simulation package for julia,” .
- [45] A. Revelli, C. C. Loo, D. Kiese, P. Becker, T. Fröhlich, T. Lorenz, M. Moretti Sala, G. Monaco, F. L. Buessen, J. Attig, M. Hermanns, S. V. Streltsov, D. I. Khomskii, J. van den Brink, M. Braden, P. H. M. van Loosdrecht, S. Trebst, A. Paramakanti, and M. Grüninger, *Phys. Rev. B* **100**, 085139 (2019).
- [46] G. Grosso and C. Piermarocchi, *Phys. Rev. B* **51**, 16772 (1995).
- [47] Y.-C. Liu, F.-C. Zhang, T. M. Rice, and Q.-H. Wang, *npj Quantum Materials* **2**, 12 (2017).
- [48] M. E. Sorensen and I. R. Fisher, *Phys. Rev. B* **103**, 155106 (2021).